Phase locking of long Josephson junctions

N. F. Pedersen* and A. Davidson
IBM Thomas J. Watson Research Laboratory, Yorktown Heights, New York 10598
(Received 26 April 1989)

We present numerical simulations on the phase locking of solitons in long Josephson junctions by the application of external microwave signals. The full partial differential equation with boundary conditions has been used. Overlap and inline geometries are considered; the effects of dc magnetic fields and different configurations of the rf field have also been investigated.

I. INTRODUCTION

Recent experiments[1-3] on the phase locking of long Josephson junctions have increased the interest in the topic. The phase locking observed experimentally has been of two different types; in one case the long Josephson junction (LJJ) is locked to an external rf signal,[1,3] and in the other case two or several LJJ's are mutually locked.[2] In this latter case a large amount of radiated microwave power was observed (about 0.2 μW at 10 GHz), so the topic clearly has technological significance. There has been some recent theoretical work[4] aimed at obtaining an understanding of a LJJ phase locked to an rf signal; this semianalytical model, in which the soliton has particle-like properties, provides rather simple expressions for the dynamics and the range of phase locking. Other work[5] uses the multimode expansion technique to obtain approximate solutions to the perturbed sine-Gordon equation (PSGE). In this paper we have used the necessary computer time and performed a full numerical simulation of the PSGE with boundary conditions. Our results are compared to those of the semianalytical particle model, and similarities and differences are pointed out.

The paper is organized in the following way. Section II describes the equations, the numerical methods, and the criteria for the characterization of the different types of solutions. Section III and several subsections show the results of the simulations for overlap junctions, including the locking range and the effect of a dc magnetic field. Section IV shows the corresponding results for junctions of inline geometry. Section V discusses the results and concludes the paper.

II. THE EQUATIONS, NUMERICAL METHODS, AND CHARACTERIZATION OF SOLUTIONS

A. The equation

The long Josephson junction is described by the perturbed sine-Gordon equation given by[6,7]

$$-\phi_{xx}+\phi_{tt}+\alpha\phi_t+\sin\phi=\eta\ . \tag{1}$$

Here time t is normalized to the inverse plasma frequency $1/\omega_0=(\hbar C/2eJ_0)^{1/2}$, where C is the capacitance per unit area and J_0 is the pair current density. The spatial dimension x is measured in units of the Josephson penetration depth, $\lambda_\sigma=(\hbar/2e\mu_0 dJ_0)^{1/2}$. η is the (normalized) external bias current, which may be space and time dependent, and the damping constant α is given by $\alpha=(\hbar/2er^2J_0C)^{1/2}$, where r is the tunneling resistance per unit area.

Since r scales inversely with the area and J_0 and C are proportional to the area, α is a quantity determined only by the properties of the barrier. Finally $\phi(x,t)$ is the phase difference between the superconducting pair phases on either side of the junction. Equation (1) is known to support the motion of solitons—or fluxons, as they are called in the present system.[6,7] The fluxon (a quantum of magnetic flux) is a 2π phase shift that may move along the junction length under the competing influence of the bias current and the damping. An approximate analytical expression for the fluxon is

$$\phi=4\tan^{-1}(e^{\xi}) \tag{2}$$

with $\xi=(x-ut)\gamma(u)$. Here $\gamma(u)$ is the Lorentz factor defined by $\gamma(u)=(1-u^2)^{-1/2}$. u is the fluxon velocity, which in normalized units has a maximum value of 1. The normalized voltage connected with Eq. (2) is

$$\phi_t=2u\sin(\phi/2)\ , \tag{3}$$

which appears as a propagating voltage pulse on the Josephson transmission line (JTL). The detailed dynamics of the fluxon will critically depend on the parameter values, and on the boundary conditions, which will be introduced as they are needed for the particular problems to be considered.

B. Numerical methods

We solved Eq. (1) with boundary conditions discussed later, by a fourth-order Runge-Kutta time integration. The spatial derivatives were approximated by simple finite differences between segments of the discretized junction. This method is equivalent to integrating a second-order differential equation for each segment of the junction. We scaled the segment so that there were at least 20 within a Josephson penetration depth. Most of the data reported here used 241 segments in a line 12 penetration lengths long. We found a time step of 0.0126 normalized units (500 steps per rf cycle), sufficient to

maintain convergence of the integration.

Our use of finite differences for the spatial derivatives means that our solutions correspond to a line of discrete junctions coupled by lumped inductors. However, the use of 20 such segments per penetration depth makes the results acceptably accurate.

C. Characterization of solutions

The topic of our paper may be illustrated by a typical example of a numerical simulation as shown in Fig. 1. It displays the voltage ϕ_t as a function of space x and time t. The parameters are $l=12$, $\alpha=0.1$, $\eta=0.155$ (overlap geometry as defined in Sec. III). For the boundary conditions (with applied rf signal) we have used

$$\phi_x(0,t)=\phi_x(l,t)=\kappa_{\rm rf}\sin\omega t \ , \tag{4}$$

with $\kappa_{\rm rf}=0.4$ and $\omega=0.214$.

The details of the boundary conditions and the parameter choice will become clear in the following sections, and Fig. 1 is just meant to illustrate the methods we are using for the analysis. The dynamics shown in Fig. 1 is simple. The voltage of the soliton, ϕ_t, is pulselike. It travels in one direction as a soliton and in the other as an antisoliton. The periodic energy input to both boundaries (as described in Refs. 7 and 8), which is a consequence of the boundary condition Eq. (4), will be in synchronism with the external rf field at frequency ω, if the following condition is satisfied:

$$\Delta T=2l/u_{\rm av}=2\pi/\omega \ . \tag{5}$$

Here ΔT is the time between two successive collisions of the soliton with the same end of the junction (see Fig. 1), and $u_{\rm av}$ is the average soliton velocity. Our numerical test for this phase locking consists of a spatial Poincaré map. That is, we plot ϕ_t (or alternatively ϕ_x or ϕ) once for every full rf cycle, i.e., at time intervals $\Delta T=2\pi/\omega$. If phase locking has occurred, the corresponding ϕ_t curves should be identical and will be plotted on top of each other. (This is a simple extension of the Poincaré map for a usual driven ordinary differential equation.) Under some circumstances subharmonic locking may occur. In this case the soliton line shape repeats itself exactly after a number, N, of full rf cycles. Figure 2 shows such an example with the spatial Poincaré map for a period 3 subharmonic ($N=3$). Figure 2 shows the results

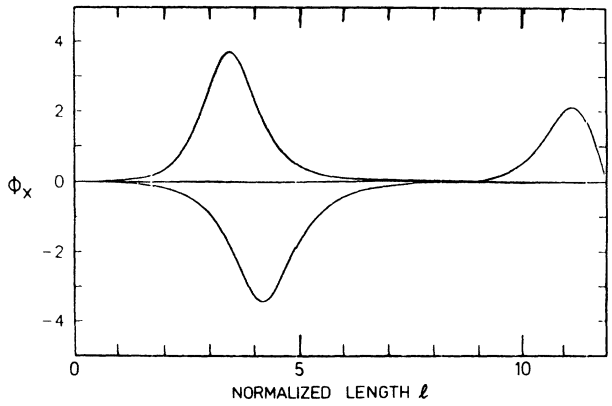

FIG. 2. Spatial Poincaré map for a period 3 phase-locked solution—overlap junction: $l=12$, $\eta=0.22$, $\alpha=0.1$, $\omega=0.642$, and $\kappa_{\rm rf}=0.4$.

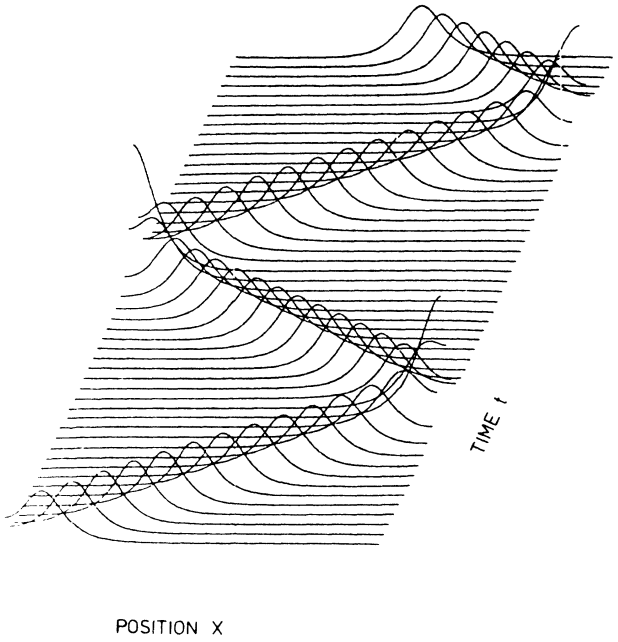

FIG. 1. Soliton phase locking in an overlap junction: $l=12$, $\eta=0.155$, $\alpha=0.1$, $\omega=0.214$, and $\kappa_{\rm rf}=0.4$.

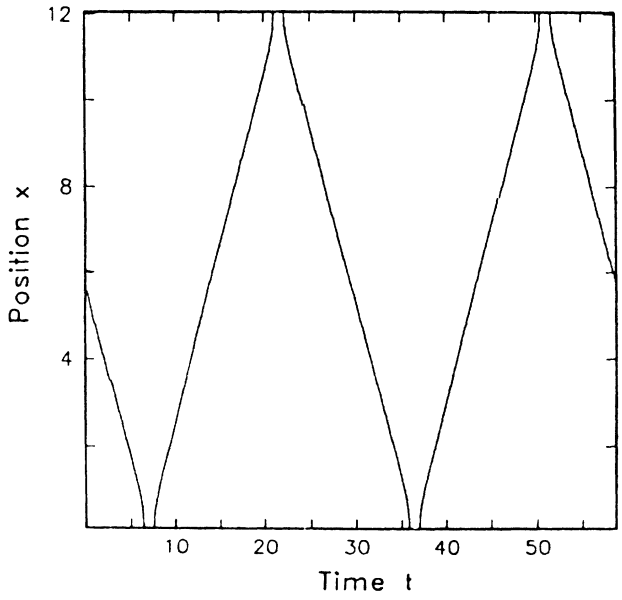

FIG. 3. Trajectory of phase-locked soliton—overlap junction: $l=12$, $\eta=0.155$, $\alpha=0.1$, $\omega=0.214$, and $\kappa_{\rm rf}=0.4$.

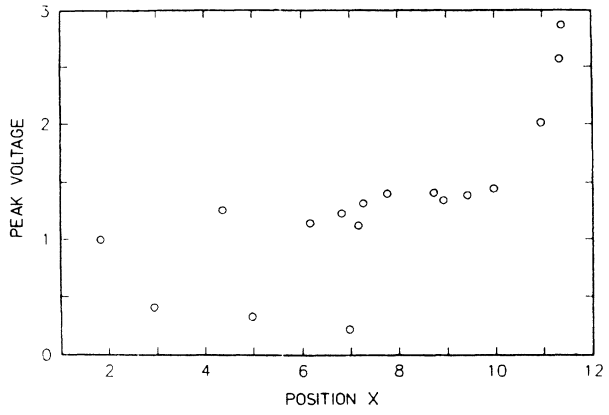

FIG. 4. Special Poincaré map as defined in the text. Inline junction with chaos: $l=12$, $\kappa_{dc}=0.7$, $\alpha=0.1$, $\eta=0$, $\omega=0.205$, and $\kappa_{rf}=0.4$.

corresponding to plotting 12 rf cycles after the initial transient had died out. Note that for clarity we have used ϕ_x as the ordinate instead of ϕ_t. (ϕ_x is negative for an antisoliton.) The parameters are as in Fig. 1, except $\eta=0.22$ and $\omega=(3)\ 0.214=0.642$. To simplify the study of soliton dynamics we also developed a useful subprogram to record the instantaneous peak voltage and plot this as a function of time and position in the junction. Thus we can obtain the trajectory of the "particle" corresponding to the soliton. Figure 3 shows an example of such a plot with parameters corresponding to those of Fig. 1. The anomalies at the junction ends are due to details of the collisions with the boundaries. (Energy absorption and phase shift occur in the collision process.[7,8])

Yet another type of test—somewhat like a Poincaré map—is shown in Fig. 4. Here the peak voltage and the position corresponding to that peak voltage are sampled once every rf cycle at time intervals $\Delta T=2\pi/\omega$. Figure 4 shows such a plot for a case in which chaotic intermittent motion has occurred. (This type of motion for a so-called inline junction will be discussed in more detail in Sec. IV.) Figure 4 has the following parameters: $l=12$, $\alpha=0.1$, $\omega=0.205$, and $\eta=0$. The boundary conditions are $\phi_x(0,t)=0.7+0.4\ \sin\omega t$ and $\phi_x(l,t)=-0.7+0.4\sin\omega t$.

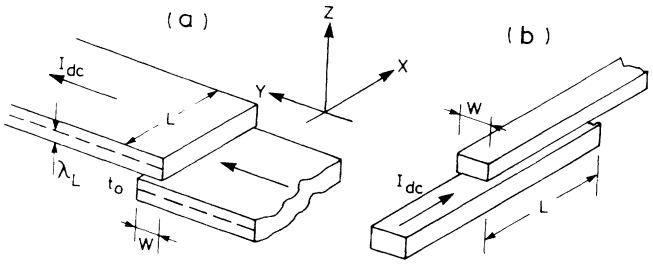

FIG. 5. Geometry of the overlap (a) and inline (b) Josephson junctions.

III. OVERLAP JUNCTIONS

The geometry of the overlap junction is shown in Fig. 5(a). In the absence of a magnetic field or rf excitations the boundary conditions are[6,7]

$$\phi_x(0,t)=\phi_x(l,t)=0\ . \tag{6}$$

With a dc magnetic field H_{ext} the boundary conditions are

$$\phi_x(0,t)=\phi_x(l,t)=\kappa_{HE}\ , \tag{7}$$

where $\kappa_{HE}=H_{ext}/\lambda_J J_0$, and J_0 is the maximum supercurrent density.

We will assume that the rf excitation is coupled to the LJJ through the magnetic field, H_{rf}, at the junction ends. In this case the boundary conditions may be written ($\kappa_{rf}=H_{rf}/\lambda_J J_0$) (Ref. 7)

$$\phi_x(0,t)=\phi_x(l,t)=\kappa_{rf}\sin\omega t\ . \tag{8}$$

We will assume a spatially uniform bias current in Eq. (1). Thus we have $\eta=I_{dc}/J_0LW$, where L and W are the length and width of the LJJ, respectively, and I_{dc} is the dc bias current. $\eta=1$ corresponds to having the maximum supercurrent $I_0=J_0LW$.

A. Range of phase locking: overlap geometry

One of the important quantities to determine is the range of phase locking, i.e., the range of bias current, $\Delta\eta$, for which the LJJ remains phase locked. This of course depends on the rf amplitude, κ_{rf}, and possibly other factors as well. In Ref. 1 it was found experimentally that $\Delta\eta$ was proportional to κ_{rf}. This same behavior was also

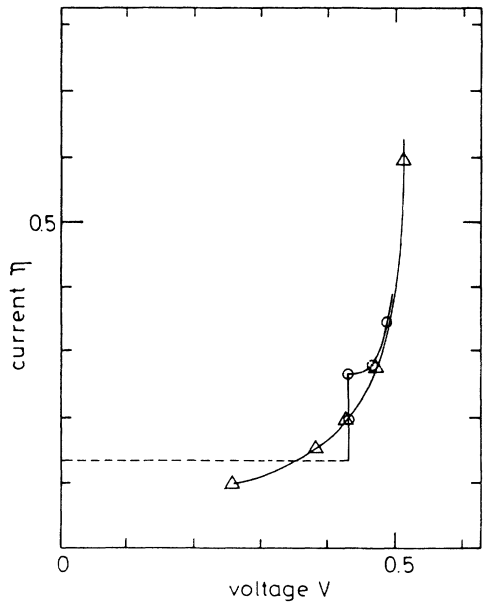

FIG. 6. *IV* curve of overlap junction: $\alpha=0.1$, $l=12$, (a) free running and (b) rf driven with $\omega=0.214$, $\kappa_{rf}=0.4$.

observed both experimentally and theoretically in recent papers.[3,4] Also in small area Josephson junctions[6] such behavior is most commonly observed for phase locking. Figure 6 shows a calculated IV curve for a LJJ of the overlap geometry. The parameters are $l=12$, $\alpha=0.1$, $\kappa_{rf}=0.4$, and $\omega=0.214$. The voltage is given by

$$V=\Delta\phi/\Delta t=2\pi/(l/u_{av})=(2\pi/l)u_{av} . \quad (9)$$

According to Eq. (5) phase locking has occurred if $\omega=\pi u_{av}/l$, i.e., at the fundamental phase-locking step we have a voltage $V=2\omega$. Figure 6 shows both the IV curve in the absence of an rf excitation and that with the applied rf signal. Both curves were obtained through a full numerical simulation of the partial differential equation, Eq. (1), with appropriate boundary conditions, Eqs. (6) and (8). The vertical asymptote $v=2\pi/l$ is obtained by setting $u_{av}=1$ in Eq. (9). Figure 7 shows the range of phase locking as a function of κ_{rf}. Note the linear dependence as also observed in Refs. 1, 3, and 4.

The mechanism for the phase locking is the following: Suppose the bias current is lower than $\eta=0.20$, which corresponds to the center of the step in Fig. 6. With η lower than that corresponding to the center of the step, the free running velocity is such, that after a back and forth crossing of the soliton, the external rf field has already fulfilled one period. Thus, the free running soliton must have its average velocity increased by the rf field in order to be synchronized to it. Accordingly, when the soliton is at $x=l$, it receives an energy input from the rf signal to increase its velocity. When the junction is again at $x=l$ it will arrive in phase with the rf signal to receive a new energy input; note that at $x=0$ the rf excitation is in opposite phase, but since at $x=0$ we have an antisoliton, it will also receive an energy input there.

Altogether the rf drive increases the average velocity of the soliton and keeps it phase locked. The same type of argument applies for the slowing down of the soliton when η is above the value corresponding to center of the step.

The mechanism described above is the reason that we cannot expect a phase locking when the frequency is doubled and other parameters remain unchanged. This was confirmed in our numerical simulations. When the frequency was tripled to $\omega=0.642$, we found again phase locking (cf. Fig. 2). In fact our simulations showed that the locking range was exactly the same as with $\omega=0.214$.

Figure 7 also shows the result of a simple perturbation analysis.[4] If we assume with Ref. 8 the approximation that it is the total current that is important for the dynamics, rather than the details of the spatial distribution, we may write

$$\eta l+2\kappa=\text{const} . \quad (10)$$

This leads to a simple estimate of the locking range, $\Delta\eta$, given by

$$\Delta\eta=2\kappa_{rf}l , \quad (11)$$

which is shown as the dashed-dotted lines in Fig. 7. Note that for the numerical simulation the locking range is linear with the rf amplitude for small amplitudes, and that the simple expression, Eq. (11), is a surprisingly good approximation.

In the low-bias end of the locking range, annihilation of the soliton from the bottom of the phase-locked step is very likely to occur; this leads to a zero-voltage solution. In order to precisely determine the lower part of the locking range, one must be very careful with the initial condition for the simulation, and change parameters only in small increments. This is different from the particle model[4] where the soliton number is a conserved quantity. In fact in the work of Ref. 4 it was found, that at low-bias current and parameters comparable to ours, the (conserved) soliton goes typically through a period-doubling bifurcation leading to chaos, as the bias current is reduced from the bottom of the phase-locked step.

The kinetics of the phase locking may be understood from the composite graph in Fig. 8. In the upper part is shown the phase-locked soliton (ϕ_x is displayed for convenience) on the line of length l after the transient has died out. Thus each curve consists of many retraces in synchronism with the external rf signal, i.e., at times

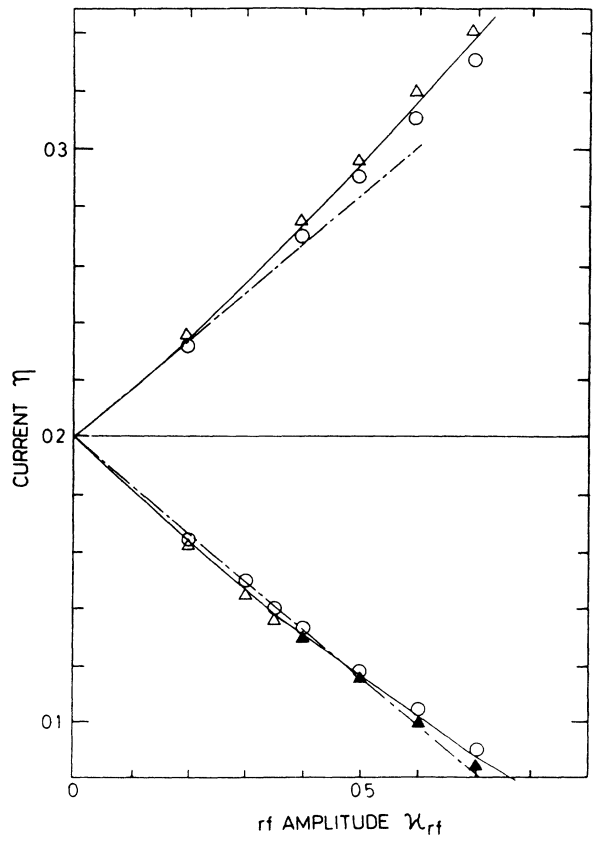

FIG. 7. Range of phase locking—overlap junction, step at $v=0.428$. $l=12$, $\alpha=0.1$, and $\omega=0.214$. Open circles correspond to phase-locked motion, open triangles to quasiperiodic behavior, and filled triangles to soliton absorption. Dashed-dotted curves: simple perturbation theory.

$T_n = nT$. Each curve in Fig. 8(a) corresponds to a different value of the bias current η, that can be read from Fig. 8(b). Note that the position of the soliton peak varies as the bias current is changed. This is plotted in Fig. 8(b), where the position Δx from the $x = l$ end of the junction is measured positive when ϕ_x is positive and negative when ϕ_x is negative. When $\eta = 0.20$ (near the center of the locking range, curve *C*) the soliton has its free running velocity. Note that the soliton is near $x = l$ when the microwave field $\kappa_{rf}\sin(\omega t)$ is near zero at $T_n = nT$. For curves *DEFG* the soliton is near the center of the junction when $\kappa_{rf}\sin\omega t$ is zero, i.e., near the edge when $\kappa_{rf}\sin\omega t$ is at its maximum. The energy transfer to the soliton is maximum, resulting in an increased average velocity. For curves *A* and *B*, we find similarly that energy is removed from the soliton, because the microwave field is near its minimum when the soliton is near $x = l$. Thus bias below the center of the step results in a decreased average velocity. We find that the locking range is exceeded when the soliton peak in Fig. 8(a) has moved such that $|\Delta x| > l/2$. Thus we may define a phase angle β being $\pi/2$ at the upper end of the locking range η_u where $\Delta x = l/2$ and being $-\pi/2$ at the lower end of the locking range n_L where $\Delta x = -l/2$. This is indicated in the lower part of Fig. 8(b).

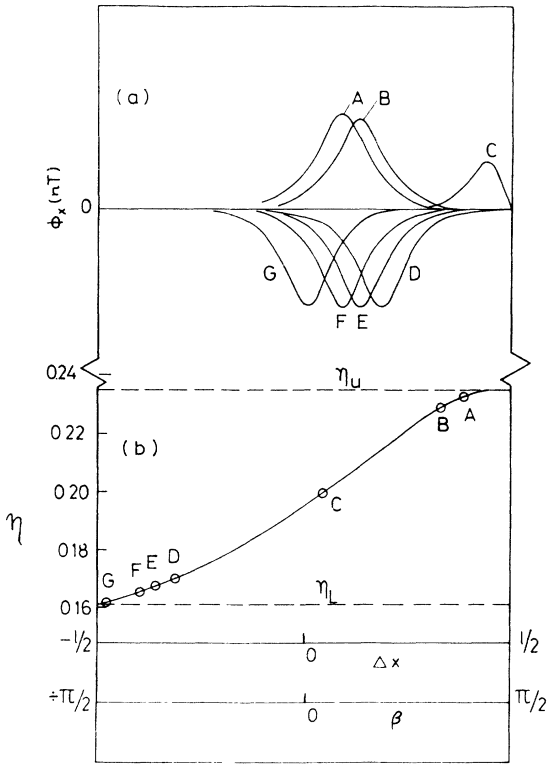

FIG. 8. Phase locking of overlap junction: $l = 12$, $\alpha = 0.1$, $\omega = 0.214$, $\kappa_{rf} = 0.2$. (a) Spatial Poincaré map: *A*: $\eta = 0.232$, *B*: $\eta = 0.23$, *C*: $\eta = 0.20$, *D*: $\eta = 0.168$, *E*: $\eta = 0.166$, *F*: $\eta = 0.164$; and *G*: $\eta = 0.162$; (b) peak position of phase-locked soliton vs bias current.

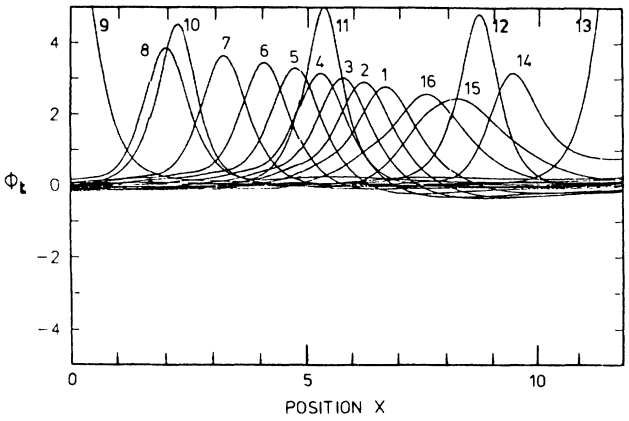

FIG. 9. Spatial Poincaré map of quasiperiodic solution—overlap junction: $l = 12$, $\alpha = 0.1$, $\eta = 0.28$, $\omega = 0.214$, $\kappa_{rf} = 0.4$. The numbering, n, corresponds to time $T_n = n2\pi/\omega$.

B. Quasiperiodic solutions

When the range of phase locking is exceeded, several different types of motion may occur. Absorption of a fluxon and subsequent transition to zero voltage happens near the lower end of the phase-locking range, η_L, in Fig. 6. At the upper end of the phase-locking range, η_u, a smooth transition to a quasiperiodic behavior takes place. The spatial Poincaré map does not repeat itself as in Fig. 2, but shows up as in Fig. 9, in which there is a new trace for every rf cycle. The numbering in Fig. 9 corresponds to strobe times defined by $T_n = n2\pi/\omega$ with $n = 1,2,3,\ldots$. Another Poincaré-like plot, which is useful to demonstrate this type of quasiperiodic behavior, is shown in Fig. 10. Here we have plotted the value of ϕ_t versus $\sin(\omega t)$, at the time when the soliton crosses the center of the LJJ going in one direction. The appearance of the plot in Fig. 10 is rather similar to a typical Poincaré map for a quasiperiodic solution to a driven ordinary differential equation (ODE).

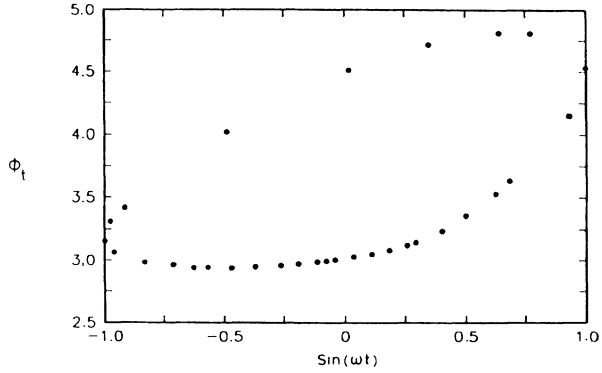

FIG. 10. Quasiperiodic solution—overlap junction: Poincaré map defined by voltage ϕ_t and time t for passing $x = \frac{1}{2}$ in one direction; $l = 12$, $\alpha = 0.1$, $\eta = 0.27$, $\omega = 0.214$, $\kappa_{rf} = 0.4$.

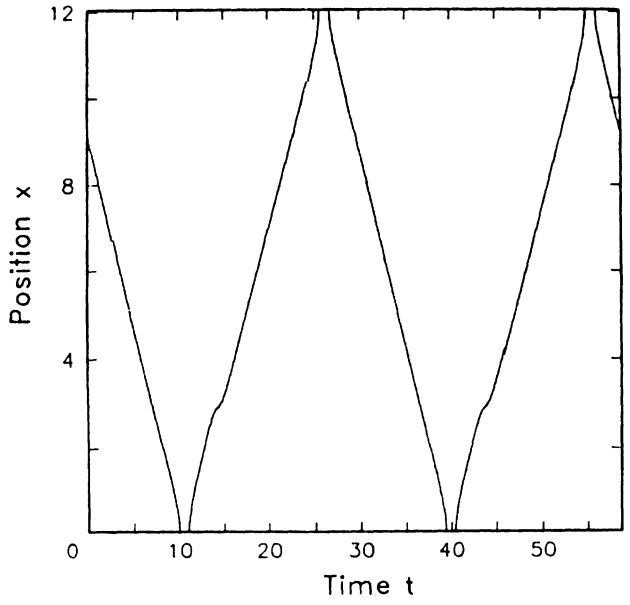

FIG. 11. Trajectory of the phase-locked soliton in a magnetic field—overlap junction: $l=12$, $\alpha=0.1$, $\eta=0.2$, $\omega=0.214$, $\kappa_{\rm rf}=0.4$, $\kappa_{HE}=0.4$.

In some cases chaos was obtained. However, a further discussion of this phenomenon will be postponed to Sec. IV which deals with inline junctions.

C. Application of a magnetic field: overlap case

The effects of a dc magnetic field, $H_{\rm ext}$, were also investigated. This was done by adding a term κ_{HE} in Eq. (8). Such a term removes the symmetry of the soliton trajectory, but phase locking is of course still possible. Figure 11 shows an example of the trajectory of a soliton phase locked to an rf magnetic field ($\kappa_{\rm rf}=0.4$, $\omega=0.214$) in the presence of a dc magnetic field ($\kappa_{HE}=0.4$). The asymmetry generated by the dc magnetic field is clearly seen in the trajectory, and for the chosen parameters the time for passing from $x=0$ to l is 14% larger than the time required for passing in the opposite direction. The bump on the trajectory is a signature of extra oscillations generated by the collision with the boundary, as will become clear later.

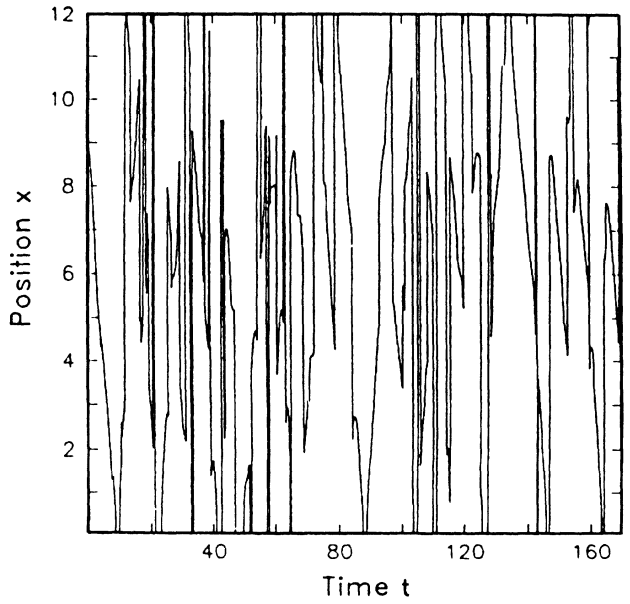

FIG. 12. Trajectory of voltage maximum—overlap junction, uniform rf excitation: $l=12$, $\alpha=0.2$, $\eta=0$, $\omega=0.7$, $\eta_{\rm rf}=0.7$.

D. Uniform rf excitation: overlap case

We also tried to investigate phase locking with a spatially uniform rf excitation in the form of a term $\eta_{\rm rf}\sin\omega t$ added to the right-hand side of Eq. (1). A somewhat similar type of investigation has been done previously in Refs. 9 and 10. We will not show the details of the calculations here, but merely summarize our results.

(1) Phase locking was very difficult to obtain, and the locking range very small—even with fairly large values of $\eta_{\rm rf}$ ($\eta_{\rm rf}\sim 0.5$). Thus a homogeneous excitation seems to be unfavorable for phase locking.

(2) When the rf drive and other conditions exceed the threshold corresponding to chaos in the small junction,[11] spatially homogeneous chaos is observed with uniform initial conditions. With soliton initial conditions also very complicated spatially inhomogeneous chaos may be observed under these circumstances.

(3) Below the threshold for chaos conversion from a soliton mode to a cavity type of excitation (standing wave) may take place.

Figure 12 shows as an example the trajectory of the peak voltage corresponding to a case of spatially nonuniform chaos with uniform rf excitation and soliton initial condition. The parameters are $\eta_{\rm rf}=0.7$, $\eta=0$, $\omega=0.7$, $\alpha=0.2$, and $l=12$. A more thorough investigation of the parameter space for such complicated behavior is outside the scope of the present paper.

IV. INLINE JUNCTIONS

The geometry of the inline junction is shown in Fig. 5(b). The soliton dynamics is described by Eq. (1) (Refs. 7 and 8) with $\eta=0$, together with the boundary conditions

$$\phi_x(0,t)=-\phi_x(l,t)=\kappa_{\rm dc}=I_{\rm dc}/2\lambda_J WJ\ , \tag{12}$$

where $I_{\rm dc}$ is the dc bias current. Thus with an applied rf magnetic field as in the overlap case, we obtain

$$\begin{aligned}\phi_x(0,t)&=\kappa_{\rm dc}+\kappa_{\rm rf}\sin\omega t\ ,\\ \phi_x(l,t)&=-\kappa_{\rm dc}+\kappa_{\rm rf}\sin\omega t\ .\end{aligned} \tag{13}$$

The soliton dynamics of the inline junction is quite different from that of the overlap junction.[7,8] For the overlap case the peak voltage is rather constant over the length of the junction. For the inline case and no rf drive, Fig. 13 shows the result of plotting the peak voltage versus position.

Note that in the perturbation model this curve is a

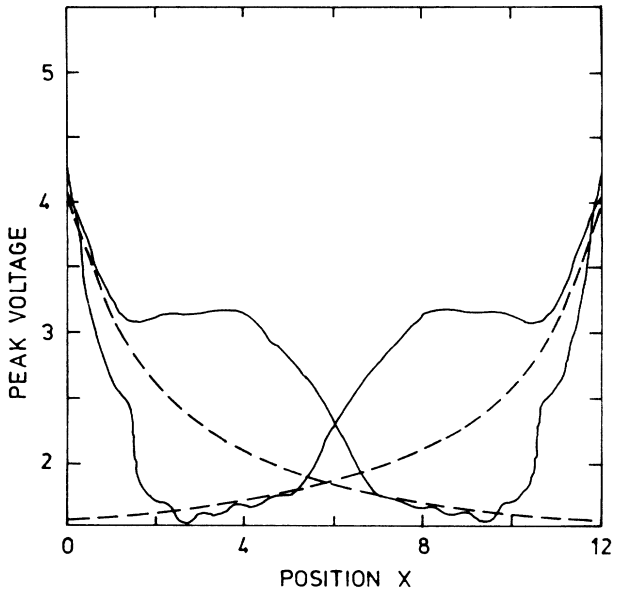

FIG. 13. Soliton (maximum) trajectory—inline junction, free running case: $l=12$, $\alpha=0.1$, $\kappa_{dc}=1.2$; dashed curve: perturbation theory qualitatively.

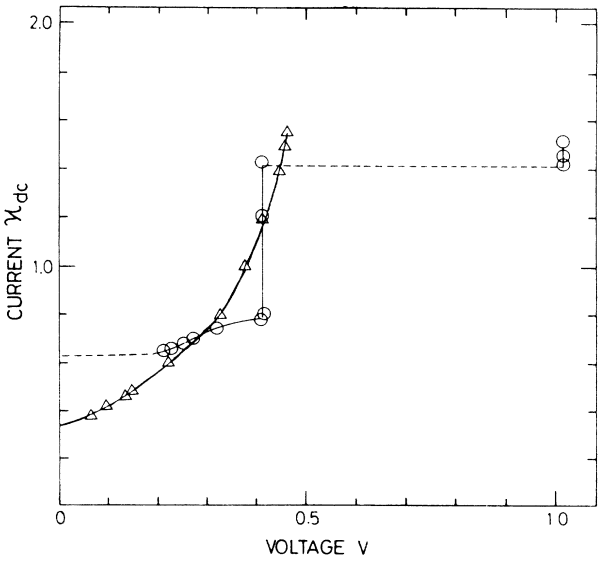

FIG. 14. *IV* curve of inline junction: $l=12$, $\alpha=0.1$; (a) free running, (b) rf driven with $\kappa_{rf}=0.4$, $\omega=0.205$.

smoothly decaying exponential[7,8] as shown qualitatively by the dashed curve. The parameters of Fig. 13 are $\kappa_{dc}=1.2$, $\alpha=0.1$, $l=12$. The plateaus seen in the computed curves have their origin in the soliton interaction with oscillations in the junction.

A. Range of phase locking: inline junction

For the inline LJJ we also calculated the *IV* curve in the presence of rf fields by numerically simulating the partial differential equation (PDE) [Eq. (1)] with appropriate boundary conditions [Eq. (13)]. Typically we used 500 time steps per rf cycle and 241 spatial segments as in the overlap case. Figure 14 shows a calculated *IV* curve with the following parameters: $\alpha=0.1$, $l=12$, $\omega=0.205$, and $\kappa_{rf}=0.4$. For $\kappa_{dc}=1.2$ the free running frequency is the same as the chosen applied frequency. The free running and phase-locked *IV* curves for the inline case appear somewhat similar to those of the overlap case (Fig. 6), although they certainly differ in details. Note for example that the phase-locked step in Fig. 14 is asymmetric. The locking range is shown in Fig. 15 as a function of κ_{rf}. Note that also for the inline geometry the phase-locking range is proportional to κ_{rf} for small κ_{rf}. Simple perturbation theory[4,8] predicts that the locking range $\Delta\kappa_{dc}=\kappa_{rf}$, which is shown as the dashed-dotted curves. At the upper end of the locking range, κ_u, the range of phase-locking falls short of the perturbation theory prediction. For κ_{rf} below ~ 0.35 we have a transition from phase locked to quasiperiodic behavior somewhat similar to that of Fig. 7. Around $\kappa_{rf}\simeq 0.35$ there is a break in the curve, which is caused by the creation of an additional soliton on the line. This may be seen from Fig. 14, where it is observed that switching takes place to a

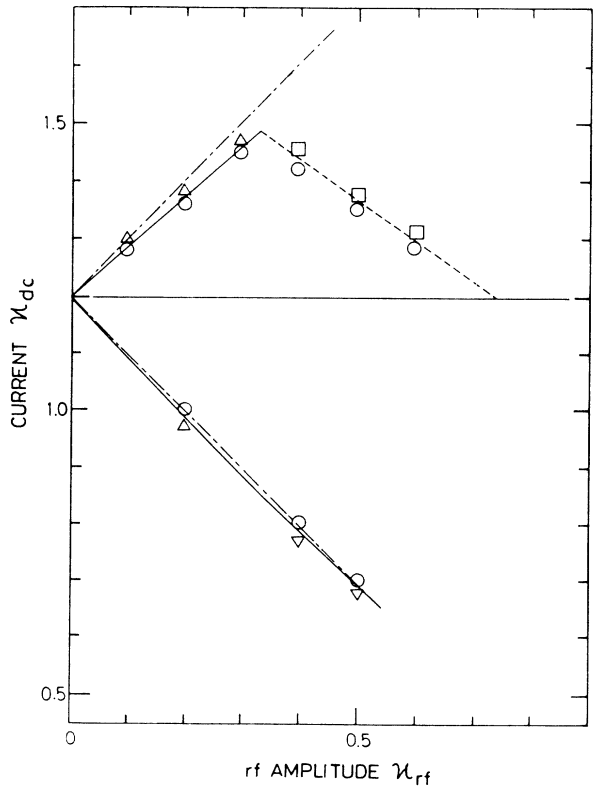

FIG. 15. Range of phase locking—inline junction: step at $v=0.41$. $l=12$, $\alpha=0.1$, and $\omega=0.205$; circles correspond to phase locking, squares to chaos, upright triangles to quasiperiodic, and upside down triangles to intermittent quasiperiodic behavior. Dashed-dotted lines: simple perturbation theory.

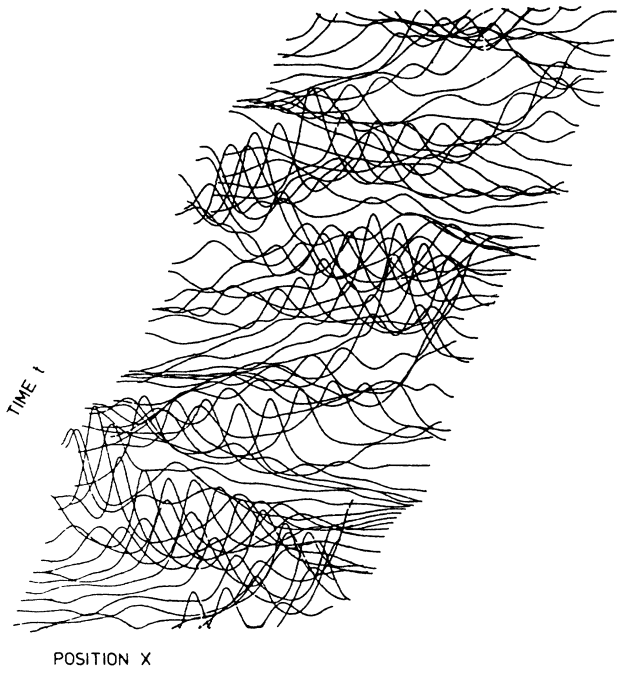

FIG. 16. Inline junction with chaos: $l=12$, $\alpha=0.1$, $\kappa_{dc}=1.452$, $\kappa_{rf}=0.4$, $\omega=0.205$.

state with $v \simeq 1.0$, approximately twice the limiting voltage of a one soliton state. Note that $\kappa_{dc}=2$ corresponds to the critical current, where fluxons and antifluxons are created continuously at the edges.[7,8] At the threshold discussed (dashed line in Fig. 15) we have approximately $\kappa_{dc}+\kappa_{rf}=1.85$. The soliton motion in the region of the parameter just above that line space is chaotic and will be discussed in the next section.

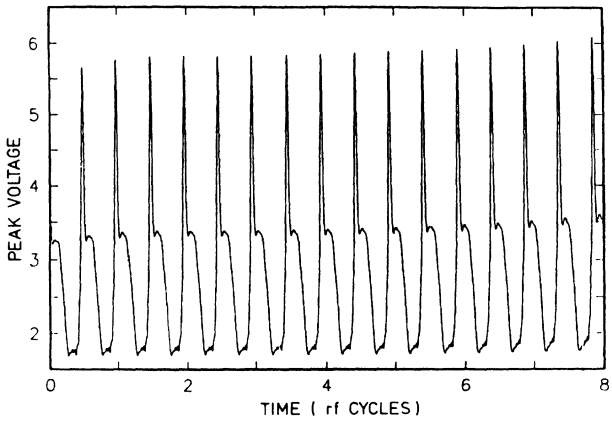

FIG. 18. Inline junction—quasiperiodic solution shown with peak voltage: $l=12$, $\alpha=0.1$, $\kappa_{dc}=1.25$, $\kappa_{rf}=0.2$, $\omega=0.205$.

B. Inline junction: chaotic solutions

The soliton motion after the threshold for the generation of a new soliton has been passed (the upper end of the locking range as discussed earlier) may best be described as chaotic, as can be seen in Fig. 16. Solitons are apparently continuously let in an out of the junction, but on the average there are approximately two. As noted above this is in agreement with the voltage of approximately 1.0 as observed in Fig. 14 for $1.42<\kappa_{dc}<1.58$. Figure 17 displays this type of solution in another way. Here the peak voltage is plotted as a function of position in the junction for a number of rf periods. Again the solution is by appearance clearly chaotic. A further study of this type of complicated motion is outside the scope of this paper, and will be left for later investigations.

At the lower rf amplitudes, where new solitons are not created, the quasiperiodic motion may typically appear as

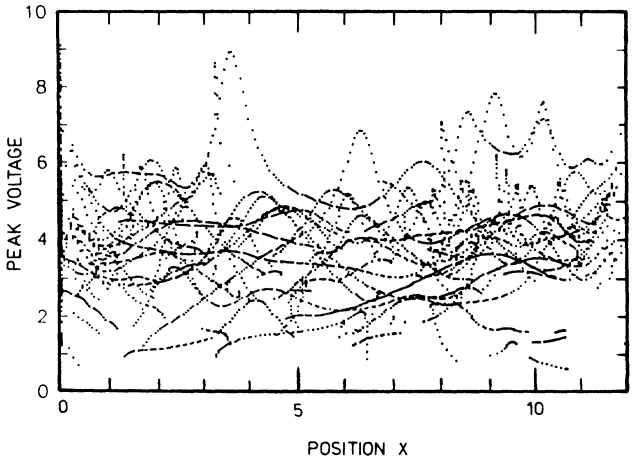

FIG. 17. Peak voltage as a function of position-inline junction, chaos: $l=12$, $\alpha=0.1$, $\kappa_{dc}=1.55$, $\kappa_{rf}=0.4$, $\omega=0.205$.

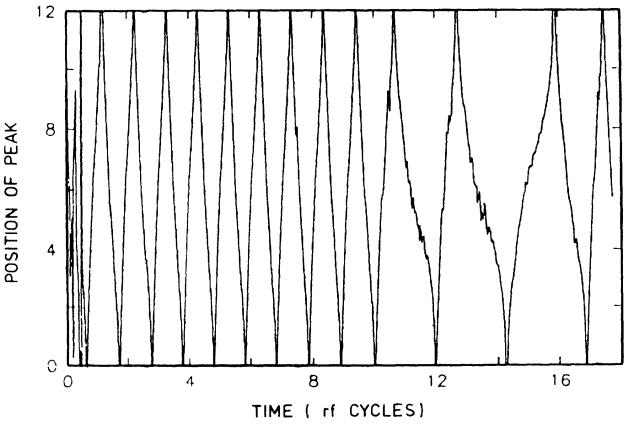

FIG. 19. Inline junction—trajectory of intermittent soliton motion: $l=12$, $\alpha=0.1$, $\kappa_{dc}=0.75$, $\kappa_{rf}=0.4$, $\omega=0.205$.

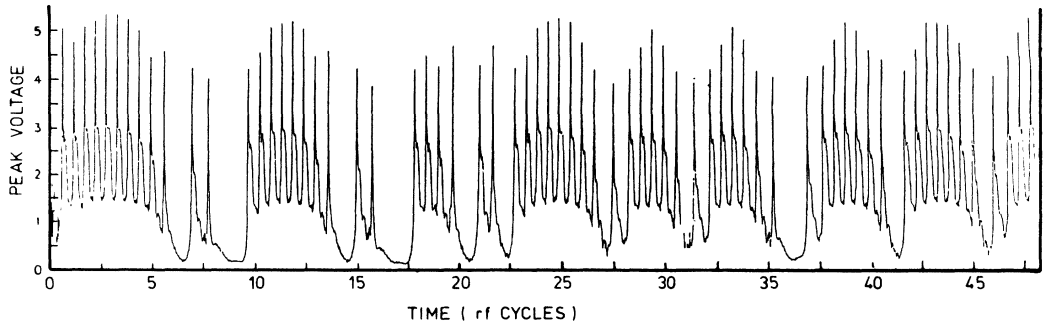

FIG. 20. Inline junction—peak voltage of intermintent, chaotic soliton motion: $l=12$, $\alpha=0.1$, $\kappa_{dc}=0.7$, $\kappa_{rf}=0.4$, $\omega=0.205$.

in Fig. 18, where we have displayed the peak voltage (cf. Fig. 13) for $\kappa_{rf}=0.2$. The signal is changing slowly because there is no phase lock. For the shown example there are 5.1 back and forth crossings of the soliton in 5.0 rf periods.

At the lower end of the locking range but for higher values of κ_{rf}, we observe another very interesting nonlinear soliton motion. Here the motion appears—for a number of rf cycles—to be quasiperiodic (almost phase locked) as in Fig. 18, but then there is a transition to a state in which the solition moves very slowly in the center of the junction—outside the reach of the rf signal. Eventually it will again reach the other end to be stimulated by the rf signal and possibly to be (almost) phase locked again. A typical peak voltage trajectory is shown in Fig. 19. Over many rf cycles the signal appears as a series of bursts at irregular intervals as seen in Fig. 20. Such a signal is typical of chaotic intermittency[12] and will be characterized by a large low-frequency noise component. The intermittency is probably stimulated by the details of the oscillations of the line in connection with the slow motion in the inside of the junction when the phase lock is lost.

V. CONCLUSION

The phase locking of solitons in long Josephson junctions by means of an external rf field has been investigated by a full numerical simulation of the partial differential equation. When appropriate, a comparison to the results of a simple perturbation approach has been made. Besides the phase-locked behavior, quasiperiodic, intermittent, and chaotic motion of the soliton has been observed.

*Permanent address: Physics Laboratory I, Technical University of Denmark, DK-2800 Lyngby, Denmark.

[1]M. Cirillo and F. L. Lloyd, J. Appl. Phys. **61**, 2581 (1987).
[2]R. Monaco, S. Pagano, and G. Costabile, Phys. Lett. A **131**, 122 (1988).
[3]G. Costabile, R. Monaco, and S. Pagano (unpublished).
[4]M. Salerno, M. R. Samuelsen, G. Filatrella, S. Pagano, and R. D. Parmentier (unpublished); Phys. Lett. A **137**, 75 (1989).
[5]G. Rotoli, *Stimulation Effects in Josephson Junctions* (World Scientific, Singapore, to be published).
[6]A. Barone and G. Paterno, *Physics and Applications of the Josephson Effect* (Wiley, New York, 1982).
[7]N. F. Pedersen, in *Solitons,* edited by S. E. Trullinger, V. E. Zakharov, and V. L. Pokrovsky (Elsevier, New York, 1986), Chap. 9.
[8]O. H. Olsen, N. F. Pedersen, M. R. Samuelsen, H. Svensmark, and D. Welner, Phys. Rev. B **33**, 168 (1986).
[9]M. Cirillo, J. Appl. Phys. **60**, 338 (1986).
[10]G. Reinisch, J. C. Fernandez, N. Flytzanis, and S. Pnevmatikos, Phys. Rev. B **38**, 11 284 (1988).
[11]N. F. Pedersen and A. Davidson, Appl. Phys. Lett. **39**, 830 (1989).
[12]H. G. Schuster, *Deterministic Chaos* (Physik Verlag, Weinheim, 1984).